Facile Synthesis of Red/NIR AIE Luminogens with Simple Structures, Bright Emissions, and High Photostabilities, and Their Applications for Specific Imaging of Lipid Droplets and Image-Guided Photodynamic Therapy

*Dong Wang, Huifang Su, Ryan T. K. Kwok, Guogang Shan, Anakin C. S. Leung, Michelle M. S. Lee, Herman H. Y. Sung, Ian D. Williams, Jacky W. Y. Lam, and Ben Zhong Tang**

Red/near-infrared (NIR) fluorescent molecules with aggregation-induced emission (AIE) characteristics are of great interest in bioimaging and therapeutic applications. However, their complicated synthetic approaches remain the major barrier to implementing these applications. Herein, a one-pot synthetic strategy to prepare a series of red/NIR-emissive AIE luminogens (AIEgens) by fine-tuning their molecular structures and substituents is reported. The obtained AIEgens possess simple structures, good solubilities, large Stokes shifts, and bright emissions, which enable their applications toward in vitro and in vivo imaging without any pre-encapsulation or -modification steps. Excellent targeting specificities to lipid droplets (LDs), remarkable photostabilities, high brightness, and low working concentrations in cell imaging application make them remarkably impressive and superior to commercially available LD-specific dyes. Interestingly, these AIEgens can efficiently generate reactive oxygen species upon visible light irradiation, endowing their effective application for photodynamic ablation of cancer cells. This study, thus, not only demonstrates a facile synthesis of red/NIR AIEgens for dual applications in simultaneous imaging and therapy, but also offers an ideal architecture for the construction of AIEgens with long emission wavelengths.

1. Introduction

Fluorescence imaging has been proven to be a highly sensitive and noninvasive technology that offers researchers a very useful tool for analytical sensing and optical imaging.[1] By utilizing fluorescence imaging, direct visualization of bioanalytes could be achieved on site and in time, and useful insights into complex biological structures and processes could be straightforwardly provided.[2] In particular, fluorophores with intense emission in the red/near-infrared (NIR) region are nowadays undergoing an explosive development in biological applications, owing to their capabilities of overcoming the interference of optical absorption, reducing light scattering, avoiding autofluorescence of physiological environments, as well as minimizing photodamage to biological structures.[3] Although many types of red/NIR-emissive fluorophores have been commercialized, current situation is still far from ideal. Conventional red/NIR-emissive fluorophores generally suffer from a common photophysical phenomenon notoriously named as aggregation-caused quenching (ACQ).[4] Conventional fluorophores emit strongly in solution phase; however, they experience emission quenching upon aggregates formation due to intermolecular π–π stacking and other nonradiative pathways. For examples, some commercial bioimaging dyes including MitoTracker Red, ER-Tracker Red, LysoTracker Deep Red, and Nile Red are all brightly red emissive in diluted dimethyl sulfoxide

Dr. D. Wang, Dr. H. Su, Dr. R. T. K. Kwok, Dr. G. Shan, A. C. S. Leung, M. M. S. Lee, Dr. H. H. Y. Sung, Prof. I. D. Williams, Dr. J. W. Y. Lam, Prof. B. Z. Tang
Department of Chemistry
Hong Kong Branch of Chinese National Engineering Research Center for Tissue Restoration and Reconstruction
Institute of Molecular Functional Materials
State Key Laboratory of Neuroscience
Division of Biomedical Engineering and Division of Life Science
The Hong Kong University of Science and Technology
Clear Water Bay, Kowloon, Hong Kong, China
E-mail: tangbenz@ust.hk

The ORCID identification number(s) for the author(s) of this article can be found under https://doi.org/10.1002/adfm.201704039.

DOI: 10.1002/adfm.201704039

Prof. B. Z. Tang
Guangdong Provincial Key Laboratory of Brain Science Disease and Drug Development
HKUST-Shenzhen Research Institute
No. 9 Yuexing 1st RD, South Area, Hi-tech Park, Nanshan
Shenzhen 518057, China

Prof. B. Z. Tang
Guangdong Innovative Research Team
SCUT-HKUST Joint Research Laboratory
State Key Laboratory of Luminescent Materials and Devices
South China University of Technology
Guangzhou 510640, China

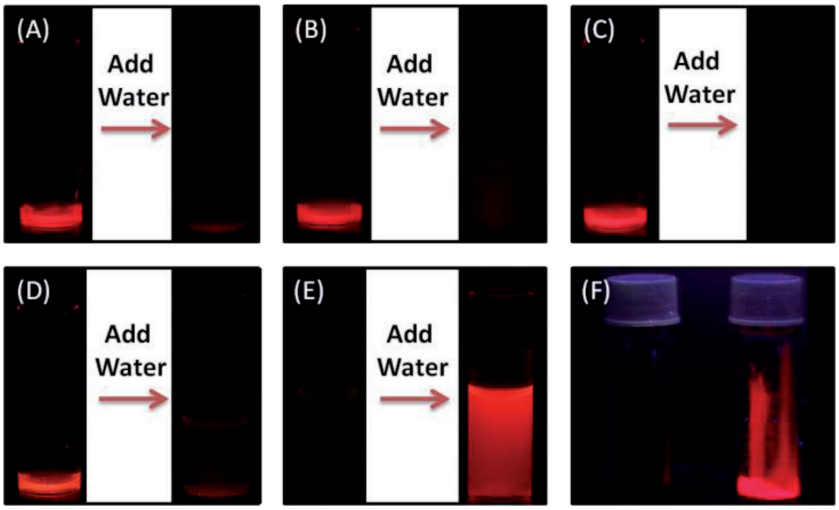

Figure 1. ACQ versus AIE. ACQ phenomenon of conventional dyes: A) ER-Tracker Red, B) MitoTracker Red, C) LysoTracker Deep Red, and D) Nile Red. E) AIE phenomenon of AIEgen TPMN. F) Fluorescence photographs of Nile Red (left) and AIEgen TPMN (right) in the solid state taken under 365 nm UV irradiation.

solutions, but the emissions are partially or totally quenched upon the formation of aggregates after adding water (**Figure 1**A–D, Table S1, Supporting Information). In particular, as illustrated in Figure 1F, Nile Red is almost nonemissive in solid state. The fluorescence photographs in Figure 1 clearly demonstrate that ACQ phenomenon leads to low photobleaching resistance; thus, this would greatly impede the practical applications in the area of biomedical research, since conventional fluorophores tend to form aggregates in physiological environments or aqueous media due to the high hydrophobicity of their emitting centers with planar conformations. We have developed a novel class of fluorophores with twisted conformations exhibiting extraordinary aggregation-induced emission (AIE) feature,[5] which is completely opposite to ACQ dyes. These compounds with AIE characteristics are nonemissive or weakly emissive in solutions but are induced to florescent intensely in aggregates through a mechanism of the restriction of intramolecular motions, resulting in intrinsic capability to work perfectly at high concentrations or in aggregation state with bright fluorescence (as shown in Figure 1E,F) and a high photobleaching threshold. Therefore, AIE has opened a venue to an array of possibilities with great potential for high-tech innovations.[6]

Considering the great significances of both AIE and red/NIR-emission, some red/NIR-emissive AIEgens have been constructed and utilized in various biological applications.[6] Nevertheless, in general, the preparation of red/NIR fluorescent molecules is extremely complicated regardless of either the AIEgens or conventional dyes. Common synthetic strategies of red/NIR fluorophores, including connection of strong electron-donating (D) and -accepting (A) units by π-bridge(s), expansion of π-conjugation, and combination of the two strategies,[7] usually require several-step reactions and inconvenient purifications, which are extremely time-, cost-, and energy-consuming, tedious, and harmful to environment. Moreover, their applications are often restricted due to the inferior solubility resulting from their bulky structures; therefore, further fabrications or modifications with surfactants, proteins, or other materials are essentially required before biological uses. For examples, TTB[8] and TPE-TPA-DCM[9] (Scheme S1, Supporting Information) are reputable in biological applications because of their AIE characteristics, bright emissions in red region and high photostabilities, nonetheless, their synthetic procedures respectively involve seven- and six-step reactions with cumbersome and iterative purifications. In addition, efficient cellular uptake of TTB and TPE-TPA-DCM requires pre-fabrications with polyethylene glycol (PEG)-containing amphiphilic polymers or bovine serum albumin. Indeed, developing facile synthesis of red/NIR AIEgens having simple and processable structure with bright emission remains an important and challenging task with very limited success achieved even though enthusiastic efforts have been devoted by scientists.

Lipid droplets (LDs),[10] which mainly locate in adipocytes, hepatocytes, adrenal cortex, and myocytes, have been proven to be considerably important in various biofunctions, such as regulations of the storage and metabolism of neutral lipids, protein degradation, construction and maintenance of membrane, and signal transduction.[11] The abnormality of LDs in cells is a critical biomarker for various diseases including cancer, obesity, fatty liver disease, hyperlipidemia, atherosclerosis, inflammation, virus infection, type II diabetes, and neurodegeneration in Alzheimer's disease.[12] Taking the intrinsic advantages of fluorescence imaging, the development of efficient fluorescent probes of LDs is highly desired. However, commercial fluorophores (such as BODIPY dyes, Nile Red, and Oil Red O) for LDs imaging have their respective and collective drawbacks. For instance, BODIPY dyes require relatively long incubation time and their small Stokes shifts affect the collection of imaging signal;[13] the specificity of Nile Red to LDs is unsatisfactory;[14] prefixation of cells is necessary when Oil Red O is employed.[15] Besides, those commercial fluorophores exhibiting ACQ property show low photobleaching resistance. In this context, a handful of LD-specific targeting AIEgens have been exploited and proven to be powerful fluorescent probes of LDs.[16] Nevertheless, both of those previously reported AIEgens and commercial fluorophores can only be used as LD-specific probes instead of further therapeutic applications. Indeed, LDs could be an ideal organelle for therapeutic applications, thanks to their fluidity and relevance with various biofunctions. Development of AIEgens with dual functions of simultaneous LD-imaging and therapy is, therefore, attractive and useful.

Herein, we report a one-pot synthetic approach to red/NIR AIEgens with simple structures and bright emissions. These AIEgens were successfully utilized as LD-specific bioprobes in cell imaging and in vivo zebrafish imaging with high photostabilities and brightness. Meanwhile, owing to the high efficiencies of reactive oxygen species (ROSs) generation, they were proven to be effective in killing cancer cells

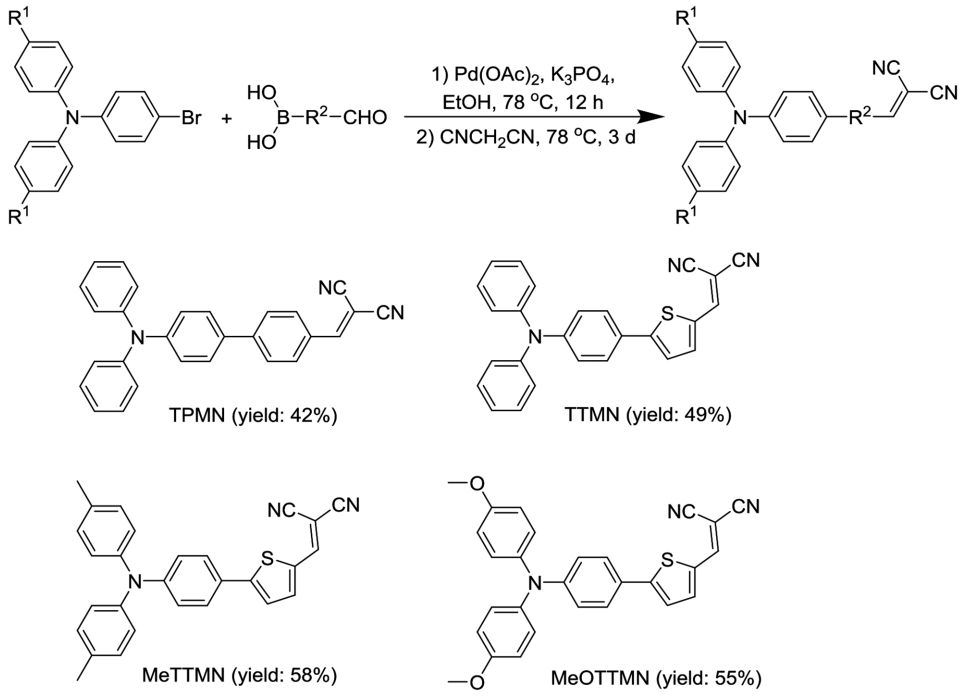

Scheme 1. One-pot synthesis of AIEgens and the structures of TPMN, TTMN, MeTTMN, and MeOTTMN.

through photodynamic therapy (PDT) process, which is gaining increasing attention on cancer treatment due to its distinct advantages, such as precise controllability, minimal invasive nature, and high spatiotemporal accuracy.[17]

2. Results and Discussion

2.1. Synthesis and Single Crystal Analysis

Taking into account the interest of cascade-reaction strategy,[18] a one-pot two-step three-component synthetic protocol was carried out through successive Suzuki–Miyaura coupling/Knoevenagel condensation reactions of substituted 4-bromo-*N*,*N*-diphenylaniline, 4-formyl aromatic boronic acid and malononitrile, in the presence of palladium catalyst using ethanol as solvent at 78 °C. Consequently, compounds TPMN, TTMN, MeTTMN, and MeOTTMN were isolated with moderate yields ranging from 42–58%, as depicted in **Scheme 1**.

Single crystals of TTMN were obtained by the slow evaporation of its solution in mixed solvents of $CHCl_3$ and hexane, endowing further study and deciphering of its optical properties and AIE behavior. As illustrated in **Figure 2**A,B, TTMN is comprised of triphenylamine segment (D), thiophene fragment (D and π-bridge), carbon–carbon double bond (π-bridge), and two cyano units (A). The molecular geometry, excluding the two phenyl rings at the end, is relatively coplanar, thus allowing good electron delocalization of the whole molecule and contributes. The ingenious combination of strong electron donor–acceptor (D-A) interaction and extended π-conjugation with good electron delocalization in this structure dose not only indicate a great potential of red emission, but also anticipate to result in an excellent push–pull system and strong excited-state intramolecular charge transfer (ICT), endowing large Stokes shift. In contrast, all the moieties

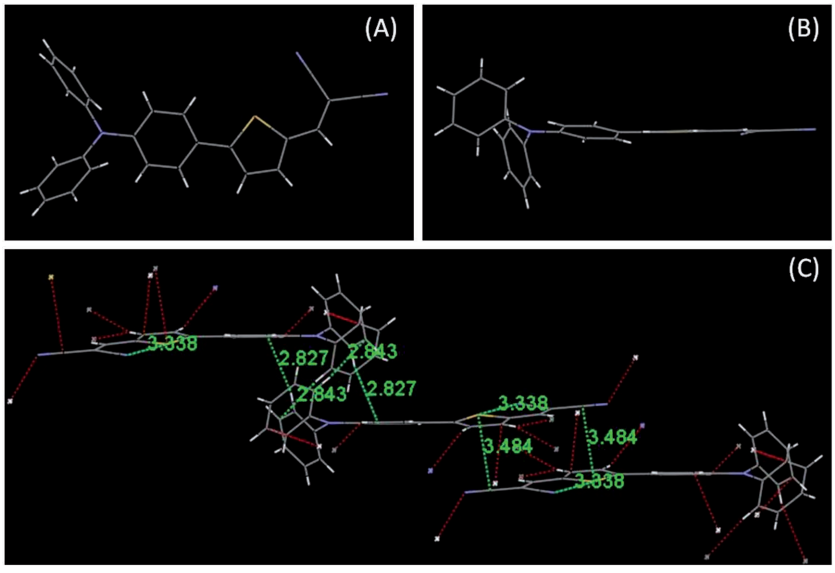

Figure 2. A) Single crystal structure of TTMN. B) Side view of the crystal structure of TTMN. C) Various inter- and intramolecular interactions in crystals of TTMN.

of TTMN could act as freely rotated molecular rotators that consume the energy of the excited state upon photoexcitation, thus ensuring that TTMN is weekly emissive in solution. Twisted conformation of triphenylamine segment extends the intermolecular distance (3.484 Å) between two parallel planes (Figure 2C), remarkably reducing the intermolecular π–π interaction, and essentially preventing emission quenching in its aggregate state. In addition, abundant inter- and intramolecular interactions (such as C—H$\cdots\pi$, C—H$\cdots$C, S$\cdots$N, and S$\cdots$C) in the crystal lattice strongly rigidify the molecular conformation and restrict molecular motions, resulting in the possibility of bright emission in the crystal state. Interestingly, the existence of intramolecular S$\cdots$N interaction may weaken undesirable twisted intramolecular charge transfer (TICT) effect, which is one of the major nonradiative pathways for the excited state to relax and deactivate, thus eventually enhancing its emissive ability.

The combination of high emission efficiency with large Stokes shift into one molecule is challenging and important for fluorescent materials. On the basis of above-mentioned results obtained from single crystal analysis of TTMN, it is believed that those synthesized compounds exhibiting interesting features, such as efficient excited-state intramolecular charge transfer, twisted conformation, and high structural rigidity, may possess the dual properties of high emission efficiency and large Stokes shift.

2.2. Photophysical Properties

Compounds TPMN, TTMN, MeTTMN, and MeOTTMN possess good solubilities in common organic solvents, such as toluene, dichloromethane, chloroform, tetrahydrofuran, acetonitrile (ACN), methanol, and dimethyl sulfoxide. Their UV–vis spectra measured in ACN are peaked at 441, 483, 492, and 499 nm, respectively, as shown in **Figure 3**A. The absorption maximums of them locate in the range of visible light, which endow less damage to biological system against UV light. The gradually redshifted absorption wavelengths can be attributed into the orderly enhanced D-A effect from TPMN to MeOTTMN. On the other hand, as depicted in Figure S5 (Supporting Information), the orderly decreased values of calculated

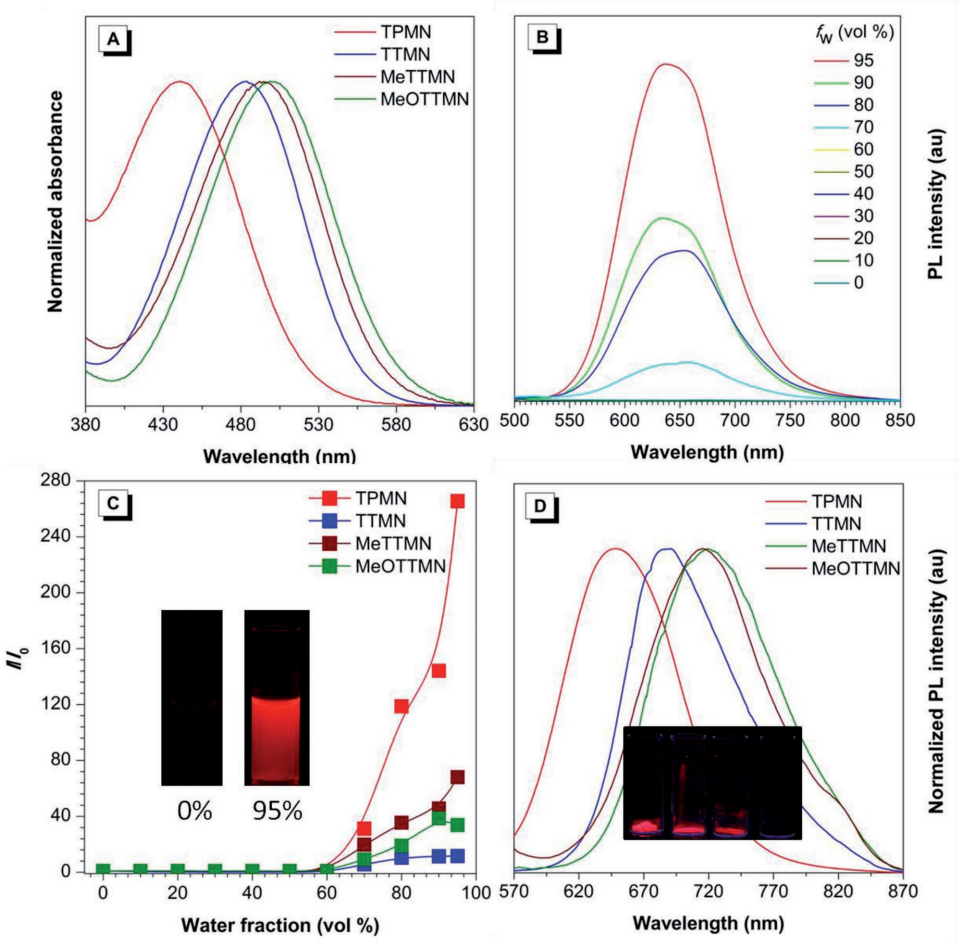

Figure 3. A) Normalized absorption spectra of TPMN, TTMN, MeTTMN, and MeOTTMN in the ACN solution. B) PL spectra of TPMN (10×10^{-6} M) in ACN/water mixtures with different water fractions (f_w); λ_{ex}: 441 nm. C) The plot of the emission maximum and the relative emission intensity (I/I_0) versus the composition of the aqueous mixture of TPMN, TTMN, MeTTMN, and MeOTTMN. Inset: fluorescence photographs of TPMN in the dilute ACN solution and in ACN/water mixtures with 95% water fractions taken under 365 nm UV irradiation. D) Normalized PL spectra of TPMN (λ_{ex}: 441 nm), TTMN (λ_{ex}: 483 nm), MeTTMN (λ_{ex}: 492 nm), and MeOTTMN (λ_{ex}: 499 nm) in the solid state. Inset: fluorescence photographs of TPMN, TTMN, MeTTMN, and MeOTTMN in the solid state taken under 365 nm UV irradiation.

energy gaps (2.565, 2.555, 2.498, and 2.405 eV) are in good accordance with experimental data of absorption maximums.

The AIE property of TPMN, TTMN, MeTTMN, and MeOTTMN was studied in ACN/water mixtures with different water fractions (f_w), which enabled certain extent of solute aggregation. In ACN solution, TPMN, TTMN, and MeTTMN weakly emit red photoluminescences (PLs) at 635, 664, and 673 nm, respectively with 0.1–0.32% of quantum yields, while MeOTTMN is nonemissive in solution state (Table S2, Supporting Information). All the four compounds show gradual increase in PL intensity with raising fraction of water starting from 70%, due to the formation of nanoaggregates that are measured and confirmed by dynamic light scattering analysis. The average hydrodynamic diameters of these nanoaggregates that formed in corresponding suspensions containing 95% fraction of water are ranging from 76.6 to 101 nm with polydispersity indexes from 0.1 to 0.22 (Figure S6, Supporting Information). The strongest PL intensities were found with 90% or 95% fraction of water upon aggregation, in which their PL intensities were enhanced to about 266-, 12-, 68-, and 34-fold comparing with those of ACN solutions (Figure 3C). Their quantum yields (18.6%, 15.8%, 7.4%, and 1.1%) in solid state also dramatically increased comparing with those in solution state. The remarkable enhancements of PL intensities in both aggregated and solid states clearly demonstrate their AIE characteristics. Their maximum emissions in aggregation state locate at 637, 672, 681, and 701 nm, indicating their red-, far red-, and NIR-emissive properties. In addition, redshifts of emissions are observed from aggregate to solid state, in which PL spectra are peaked at 648, 690, 719, and 715 nm (Figure 3D). As illustrated in Table S2 (Supporting Information), these AIEgens have extremely large Stokes shifts, even more than 200 nm. Moreover, the fluorescence decay curves of TPMN, TTMN, MeTTMN, and MeOTTMN in the solid state reveal that their lifetimes range from 0.95 to 8.32 ns (Figure S7, Supporting Information). Apparently, both long emission wavelength and bright emission of AIEgen TTMN in aggregates perfectly match the results and hypotheses that were obtained from the analysis of its single crystal. The collected photophysical data suggest that in this developed system, emissions in red/NIR region are easily tunable by fine-varying their molecular structures and substituents having different extent of D-A effect, demonstrating excellent controllability of this system in terms of emission.

To investigate the TICT effect, TTMN was chosen as an example. It was found that emission maximum of TTMN slightly redshifts from 664 to 671 nm and the emission intensity remarkably decreases with the increase of water faction at low water content in mixed ACN/water solutions (Figure S8, Supporting Information), indicating the existence of TICT effect. In fact, ACN/water is not an ideal system to study TICT effect, due to the small polarity difference. Thus, PL spectra of TTMN were recorded in different solvents with varied polarities. As depicted in Figure S9 (Supporting Information), when the solvent is changed from nonpolar toluene to polar dimethyl sulfoxide, the emission maximum largely redshifts from 573 to 665 nm, while emission intensity was considerably reduced, suggesting a strong TICT effect. Indeed, AIE properties and the TICT effect are competitive in determining the PL intensity; nevertheless, the enhanced emission feature of AIEgens in aggregates reveals a stronger AIE feature than the TICT effect in this system, reasonably benefitting from both the rigidified molecular conformation caused by powerful inter- and intramolecular interactions and restricted molecular motions in aggregates.

2.3. Bioimaging and Therapy

To evaluate the cytotoxicities of AIEgens TPMN, TTMN, MeTTMN, and MeOTTMN in living cells, 3-(4,5-dimethyl-2-thiazolyl)-2,5-diphenyltetrazolium bromide (MTT) assay was used with different concentrations of AIEgens. As illustrated in Figure S10 (Supporting Information), no significant decrease of the cell viability is observed even when the HeLa cells were cultured in the presence of 10×10^{-6} M of AIEgens for 24 h, demonstrating good biocompatibilities of these AIEgens to HeLa cells.

Cell imaging study further proceeded by employing HeLa cells as a cell model, in which the cells were pretreated with oleic acid aiming to induce considerable amount of neutral lipids. The influence of AIEgen concentration was investigated by the uses of 2×10^{-6}, 1×10^{-6}, 500×10^{-9}, and 200×10^{-9} M of TPMN. As shown in Figure S11 (Supporting Information), TPMN was strongly emissive in cells, in which the brightness did not significantly decline even the concentration was down to 200×10^{-9} M, suggesting a high brightness of TPMN in cell imaging. Colocalization experiment was then conducted by incubating HeLa cells with each presented AIEgen for 30 min and BODIPY493/503 Green for 10 min. The cell imaging of AIEgens and BODIPY493/503 Green overlapped perfectly, indicating their powerful LD-specific targeting capability (**Figure 4**). Pearson's correlation coefficients that are commonly used to determine the linear association of two variables were calculated to be up to 97% (Figure S12, Supporting Information), solidly demonstrating the high specificities of these AIEgens for staining LDs. The excellent LDs-staining specificity can be attributed to the efficiently accumulating of these lipophilic AIEgens in the hydrophobic spherical LDs which contain mainly diverse neutral lipids, such as triacylglycerol and cholesteryl ester, due to the "like–like" interactions. Moreover, as illustrated in Figure 4 and Figure S11 (Supporting Information), LDs are clearly visualized with a very high signal-to-noise ratio when relatively low concentrations (200×10^{-9} M for TPMN, TTMN, and MeTTMN, and 2×10^{-6} M for MeOTTMN) of these AIEgens were utilized. Comparing with other AIEgens used for LDs-imaging, the presented AIEgens hold the lowest working concentrations,[16] which is almost comparative to that of BODIPY493/503 Green. Interestingly, efficient cell uptake of the presented AIEgens can be achieved without any encapsulation or modification steps.

As one of the key criteria for evaluating a fluorescent bioprobe, the photostabilities of the presented AIEgens were assessed by continuous excitation and sequential scanning with confocal microscope. As depicted in **Figure 5**, for both TTMN and MeTTMN, their fluorescence intensities remain almost constant after 40 scans within 15 min irradiation, while the fluorescence intensities of TPMN and MeOTTMN keep at 84%

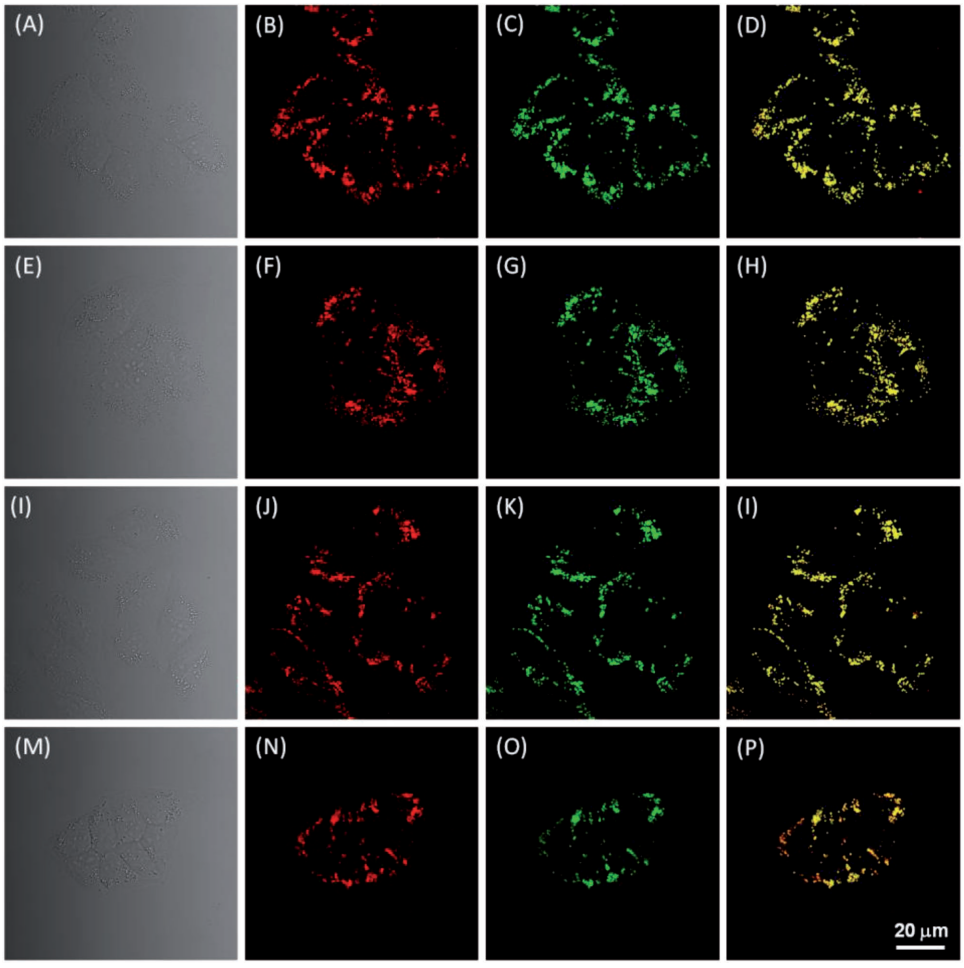

Figure 4. Colocalization imaging of HeLa cells stained with BODIPY493/503 Green and AIEgens. A,E,I,M) Bright-field and B,C,F,G,J,K,N,O) confocal images of HeLa cells stained with B) TPMN, F) TTMN, J) MeTTMN, N) MeOTTMN, and C,G,K,O) BODIPY493/503 Green. D,H,I,P) Merged images of panels (B) and (C), (F) and (G), (J) and (K), as well as (N) and (O). λ_{ex}: 488 nm (1% laser power). Concentrations: TPMN (200×10^{-9} M), TTMN (200×10^{-9} M), MeTTMN (200×10^{-9} M), MeOTTMN (2×10^{-6} M), and BODIPY493/503 Green (100×10^{-9} M). Scale bar = 20 μm.

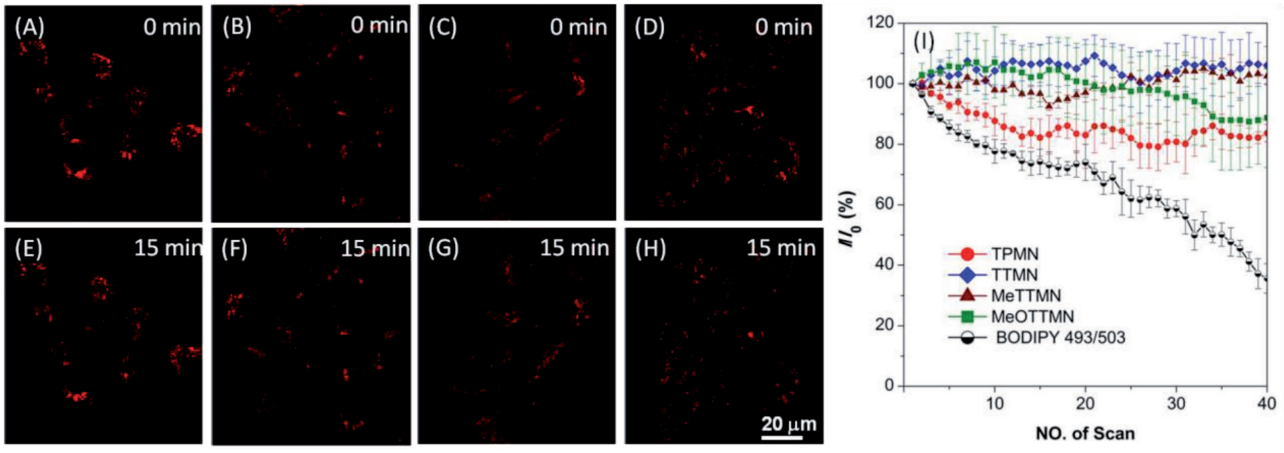

Figure 5. Confocal images of HeLa cells A–D) before (0 min, upper panel) and E–H) after the laser irradiation for 15 min (lower panel) stained with A,E) TPMN, B,F) TTMN, C,G) MeTTMN, and D,H) MeOTTMN. I) Loss in fluorescence of HeLa cells stained with AIEgens and BODIPY493/503 Green with the number of scans of laser irradiation. Concentration: 200×10^{-9} M (TPMN, TTMN, and MeTTMN), 2×10^{-6} M (MeOTTMN), and 100×10^{-9} M (BODIPY493/503 Green); λ_{ex}: 488 nm; scanning rate: 22.4 s per frame; laser power of confocal fluorescence microscope: 0.3 μW; scale bar = 20 μm.

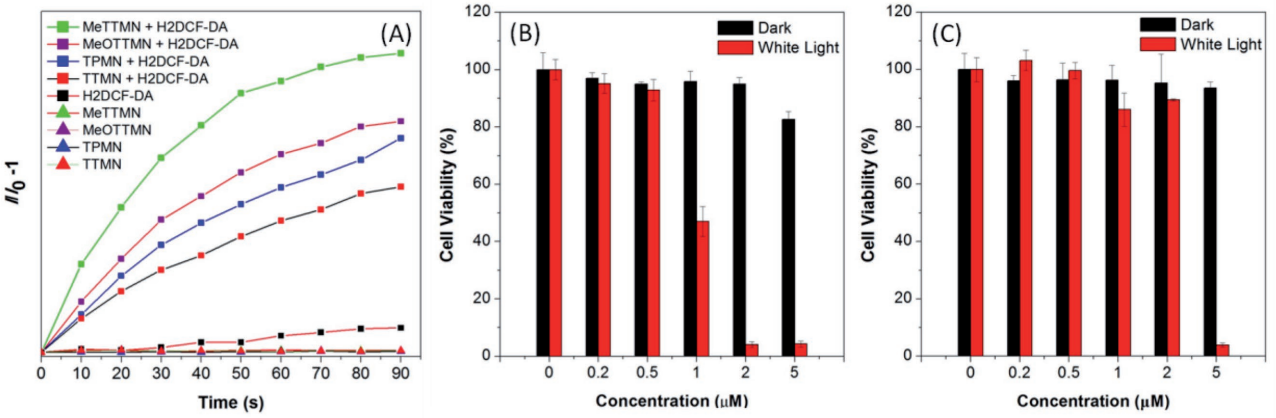

Figure 6. ROS generation upon white light irradiation and PDT study of both MeTTMN and MeOTTMN. A) Relative change in fluorescent intensity ($I/I_0 - 1$) at 534 nm of H2DCF-DA, TPMN, TTMN, MeTTMN, MeOTTMN, and mixtures of each AIEgen and H2DCF-DA in PBS upon white light irradiation for different time. Concentrations: 10×10^{-6} M (AIEgens) and 5×10^{-6} M (H2DCF-DA). Cell viability of HeLa cells stained with different concentrations of B) MeTTMN or C) MeOTTMN in the absence or presence of white light irradiation.

and 89%, respectively of its initial values in this process. By contrast, BODIPY493/503 Green suffers an obvious drop of fluorescence intensity to 35% of its initial intensity under the same conditions. Evidently, the photostabilities of these AIEgens are greatly superior to that of commercial BODIPY493/503 Green.

Apart from the application of LD-specific cell imaging, the presented AIEgens are also proven as powerful photosensitizers in ROS generation. In this experimental study, H2DCF-DA that emits fluorescence at around 534 nm triggered by ROS was employed as an ROS indicator. Considering the strong absorption of these presented AIEgens in the visible light region, white light was utilized as excitation light source. As illustrated in **Figure 6**A, in the presence of TPMN, TTMN, MeTTMN, and MeOTTMN, the emission of H2DCF-DA was gradually and rapidly intensified with the increase of irradiation time. After 90 s exposure to white light, the emission intensities of H2DCF-DA were 17, 13, 25, and 19 times higher than the original emission intensities without light irradiation, respectively. Such change, however, was not observed in AIEgens or H2DCF-DA alone under the same conditions. These results demonstrate the high ROS generation efficiencies of these AIEgens. In particular, both MeTTMN and MeOTTMN could serve as better sensitizers for ROS generation than the other two AIEgens. In this context, MeTTMN and MeOTTMN were chosen as photosensitizers to investigate the therapeutic effect of these AIEgens through PDT, which was quantitatively evaluated on HeLa cells by standard MTT assay. Both of the two AIEgens exhibit very low cytotoxicity in dark condition, regardless of the AIEgen concentration used for cell staining (Figure S10, Supporting Information and Figure 6). Low cytotoxicity in dark condition is one of the essential features of photosensitizers for PDT application. With white light irradiation, a dose-dependent toxicity is observed for both of them. In the case of MeTTMN, the HeLa cell viability decreased gradually to around 50% with concentration of 1×10^{-6} M, while increasing the concentration to 2.5×10^{-6} M eventually lead to almost complete cell apoptosis (Figure 6B). When MeOTTMN was examined, cell viability remained the same with those concentrations lower than 2.5×10^{-6} M; however, a sharp decline of cell viability was found with the concentration of 5×10^{-6} M (Figure 6C). These results clearly reveal that both of the two AIEgens are remarkably effective for killing cancer cells by PDT pathway. In addition, MeTTMN shows higher efficiency than MeOTTMN that perfectly match with the outcomes of ROS generation. Meanwhile, at the imaging concentrations of 200×10^{-9} M (MeTTMN) and 2×10^{-6} M (MeOTTMN), these two AIEgens do not cause obvious damage of cell viability even under light irradiation, making them ideal for dual applications of cell imaging and therapy through controlling AIEgen concentrations. It seems reasonable to infer that due to the fluidity and various biofunctions of LDs, the ROSs that are generated by the AIEgens with specific-targeting feather toward LDs can efficiently initiate to cell apoptosis.

Visualization of the biological structures and processes on in vivo level is of great importance.[19] However, imaging of cells in vitro by bioprobes often does not represent the real circumstances in vivo, because of the separation from native environments.[20] Encouraged by the excellent cell imaging results by using the presented AIEgens, further investigations were done for in vivo imaging of living zebrafish embryos. Zebrafish is an ideal vertebrate model for biological in vivo imaging, owing to the exceptionally high optical clarity in embryonic and larval stages. In this experiment, living zebrafish embryos were stained by these AIEgens with the concentration of 5×10^{-6} M for 30 min. As depicted in **Figure 7**, AIEgens TPMN (Figure 7G), TTMN (Figure 7H), and MeTTMN (Figure 7I) provided fluorescent images with bright red emission showing the contour profile of zebrafish. In contrast, in the case of MeOTTMN, an unclear image of zebrafish was obtained, perhaps due to its long emission wavelength located in NIR region. These preliminary results of zebrafish imaging suggest the great potential of these AIEgens for observing biological processes toward in vivo level.

3. Conclusion

In summary, we have developed a facile one-pot synthetic approach to red/NIR AIEgens with emission wavelengths

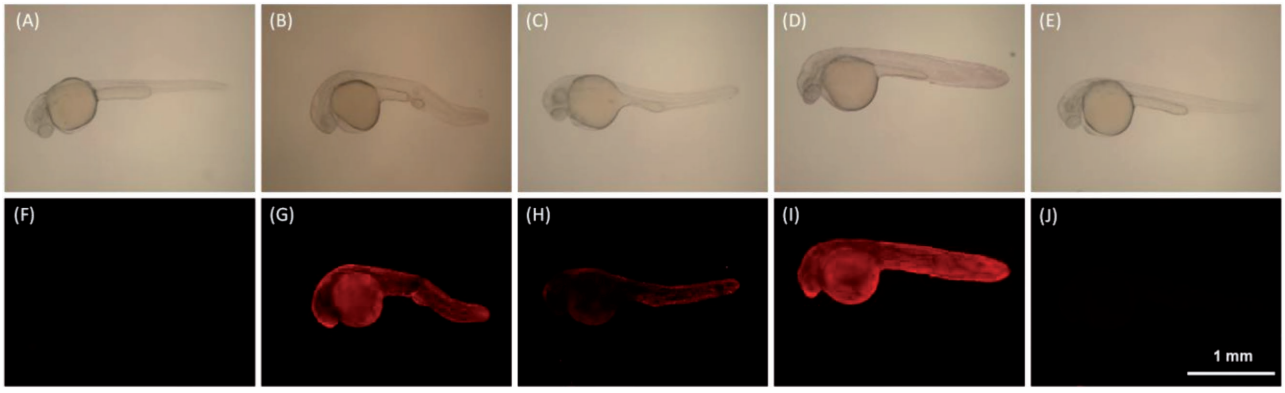

Figure 7. In vivo zebrafish imaging. A–E) Bright-field, F–J) fluorescence microscope images of living zebrafish embryos stained with B,G) TPMN, C,H) TTMN, D,I) MeTTMN, E,J) MeOTTMN, as well as A,F) images of zebrafish embryo without staining. Concentration: 5×10^{-6} M; staining time: 30 min.

ranging from 648 to 719 nm in solid state. This AIEgen system exhibits several impressive characteristics including simple structures, small molecular weights, good solubility in common organic solvents, large Stokes shifts, bright emissions, and high processabilities. These AIEgens have been proven to be considerably powerful for cell imaging, in which they show excellent LDs-targeting specificity, much higher photostability than commercial LDs-staining fluorophore, as well as high brightness even with a low concentration down to 200×10^{-9} M. These impressive properties make them as an ideal alternative of commercial LD-specific dyes. The high penetrability of these AIEgens enables the living zebrafish embryos to be brightly stained through simple incubation procedure for in vivo imaging. Moreover, with white light irradiation, their high ROS generation efficiency enables the effective application for photodynamic ablation of cancer cells, and the apoptosis of cancer cell was significantly induced by using low concentration of AIEgens. To the best of our knowledge, this would be the first report on using LD-specific AIEgens as photosensitizers for PDT application.

Our findings in this study may perfectly solve the problem of complicated synthetic procedures of red/NIR AIEgens and efficiently provide an ideal model for design, synthesis, and biological utilizations of red/NIR AIEgens. Furthermore, this study would significantly promote new strategies in the construction, modification, and functionalization of bioprobes sharing both AIE feature and long emission wavelengths on the basis of the presented system, and consequently benefit the developments of AIE study in the areas of fluorescent imaging and therapeutic applications.

4. Experimental Section

Materials: Dulbecco's Modified Essential Medium and RPMI-1640 were purchased from Gibco (Life Technologies). Ultrapure water was supplied by Milli-Q Plus System (Millipore Corporation, United States). Phosphate-buffered saline (PBS), fetal bovine serum (FBS), penicillin, streptomycin, and BODIPY 493/503 green were purchased from Thermo Fisher Scientific. H2DCF-DA was purchased from Sigma-Aldrich and used as received. 4-Bromo-*N*,*N*-diphenylaniline 4-bromo-*N*,*N*-di-*p*-tolylaniline, 4-bromo-*N*,*N*-bis(4-methoxyphenyl)aniline, (4-formylphenyl) boronic acid, (5-formylfuran-2-yl)boronic acid, and (5-formylthiophene-2-yl)boronic acid were purchased from J&K or Meryer. All the chemicals used as received without further purification.

Characterization: ^{1}H spectra were measured on Bruker ARX 400 NMR spectrometers using $CDCl_3$ as the deuterated solvent. High-resolution mass spectra (HRMS) were recorded on a Finnegan MAT TSQ 7000 Mass Spectrometer System operating in a Matrix-Assisted Laser Desorption/Ionization Time of Flight (MALDI-TOF) mode. UV absorption spectra were taken on a Milton Ray Spectronic 3000 array spectrophotometer. Steady-state fluorescence spectra were recorded on a Perkin Elmer LS 55 spectrometer. Fluorescence images were collected on Olympus BX 41 fluorescence microscope. Laser confocal scanning microscope images were collected on Zeiss laser scanning confocal microscope (LSM7 DUO) and analyzed using ZEN 2009 software (Carl Zeiss).

Cell Culture: HeLa cells were cultured in the minimal essential medium (MEM) containing 10% FBS and antibiotics (100 units mL^{-1} penicillin and 100 mg mL^{-1} streptomycin) in a 5% CO_2 humidity incubator at 37 °C.

Cytotoxicity Study: MTT assays were used to evaluate the cytotoxicity of the presented AIEgens. Cells were seeded in 96-well plates (Costar, IL, USA) at a density of 6000–8000 cells per well. After overnight culturing, medium in each well were replaced by 100 µL fresh medium containing different concentrations of the presented AIEgens. The volume fraction of dimethyl sulfoxide (DMSO) was below 0.2%. 24 h later, 10 µL MTT solution (5 mg mL^{-1} in PBS) was added into each well. After 4 h of incubation, 100 µL SDS-HCl aqueous solution (10% SDS and 0.01 M HCl) was added to each well. After incubation for 4 h, the absorption of each well at 595 nm was recorded via plate reader (Perkin-Elmer Victor3). Each trial was performed with six wells parallel.

Cytotoxicity of MeTTMN and MeOTTMN to Cancer Cells under Light Irradiation: HeLa cells were seeded in 96-well plates (Costar, IL, USA) at a density of 6000–8000 cells per well. After overnight culturing, medium in each well was replaced by 100 µL fresh medium containing different concentrations of MeTTMN or MeOTTMN. The volume fraction of DMSO is below 0.2%. After incubation for 25 min, plates containing HeLa cells were exposed to white light (around 10 mW) for 30 min, and another array of plates with cells was kept in dark as control. Then, the plates were conducted the same treatment as the biocompatibility test.

Cell Imaging: Cells were grown in a 35 mm petri dish with a coverslip at 37 °C. The live cells were incubated with certain dye at certain concentration for certain time (by adding 2 µL of a stock solution in DMSO solution to 2 mL of cell culture medium, DMSO < 0.1 vol%). After incubation with AIEgens, the cells were washed with PBS for three times. The AIEgen-labelled cells were mounted and imaged using a laser scanning confocal microscope (LSM7 DUO) at 488 nm with 1% laser power (the scanning rate was 22.4 s per frame). The emission filter was 600–744 nm.

Confocal Colocalization: For costaining with lipid dye BODIPY493/503 Green, cells were first incubated with AIEgens and BODIPY493/503 Green (100×10^{-9} M) at 37 °C for 30 min. The medium was then removed and the cells were rinsed with PBS for three times and then imaged under confocal microscope. For AIEgens, the emission filter was

600–740 nm; for BODIPY493/503 Green, the excitation was 488 nm and the emission filter was 510–553 nm.

Photostability: The dye-labeled HeLa cells were imaged by a confocal microscope (Zeiss laser scanning confocal microscope LSM7 DUO) using ZEN 2009 software (Carl Zeiss). Conditions: for AIEgens, excitation wavelength: 488 nm; for BODIPY493/503 Green, excitation wavelength: 488 nm (1% laser power).

Synthesis of Compound TPMN:[21] A dried Schlenk tube equipped with a magnetic stirring bar was charged, under a nitrogen atmosphere, with 4-bromo-*N*,*N*-diphenylaniline (162 mg, 0.5 mmol), (4-formylphenyl) boronic acid (112.5 mg, 0.75 mmol), K_3PO_4 (530 mg, 2.5 mmol), $Pd(OAc)_2$ (5.6 mg, 5 mol%), and EtOH (8 mL). The mixture was stirred at 78 °C for 12 h, after cooling down to room temperature, the reaction mixture was filtered. Then $CNCH_2CN$ (66 mg, 1 mmol) was added into the obtained filtrate, the mixture was stirred at 78 °C for another 72 h. After cooling down to room temperature, the solvent was removed under vacuum, then water (20 mL) was added into the mixture, which was extracted with CH_2Cl_2 (5 mL × 3). The combined organic phase was dried over Na_2SO_4 and filtered; the filtrate was removed under reduced pressure in order to obtain the crude product, which was further purified by silica gel chromatography (petroleum ether/CH_2Cl_2 as eluent) to yield TPMN with the yield of 42%. ^{1}H NMR (400 MHz, $CDCl_3$): 7.96 (d, J = 8.4Hz, 2H), 7.73 (t, J = 6.6Hz, 3H), 7.52 (d, J = 8.8Hz, 2H), 7.28–7.32 (m, 4H), 7.07–7.16 (m, 8H). ^{13}C NMR (100 MHz, $CDCl_3$): 159.08, 148.97, 147.08, 146.80, 131.54, 131.49, 129.46, 129.12, 127.91, 127.05, 125.13, 123.78, 122.62, 114.12, 113.01, and 80.98. ESI HRMS: calcd. for $C_{28}H_{19}N_3$ $[M]^+$: 397.1579, found: 397.1557.

Synthesis of Compound TTMN:[21] The synthetic process was similar to TPMN except for the change of starting materials. ^{1}H NMR (400 MHz, $CDCl_3$): 7.75 (s, 1H), 7.68 (d, J = 4.0Hz, 1H), 7.53 (d, J = 8.8Hz, 2H), 7.29–7.33 (m, 5H), 7.10–7.16 (m, 6H), 7.04 (d, J = 8.8Hz, 2H). ^{13}C NMR (100 MHz, $CDCl_3$): 157.11, 150.24, 149.90, 146.59, 140.36, 133.06, 129.56, 127.54, 125.48, 124.81, 124.32, 123.25, 121.67, 114.54, 113.66, and 74.99. ESI HRMS: calcd. for $C_{26}H_{17}N_3S$ $[M]^+$: 403.1143, found: 403.1150.

Synthesis of Compound MeTTMN:[21] The synthetic process was similar to TPMN except for the change of starting materials. ^{1}H NMR (400 MHz, $CDCl_3$): 7.73 (s, 1H), 7.66 (s, 1H), 7.49 (d, J = 8.8 Hz, 2H), 7.30 (s, 1H), 6.96–7.13 (m, 10H), 2.34 (s, 6H). ^{13}C NMR (100 MHz, $CDCl_3$): 157.52, 150.29, 150.20, 143.98, 140.45, 134.21, 132.79, 130.19, 127.48, 125.66, 123.88, 122.97, 120.42, 114.66, 113.76, 74.55, and 20.89. ESI HRMS: calcd. for $C_{28}H_{21}N_3S$ $[M]^+$: 431.5570, found: 403.1431.

Synthesis of Compound MeOTTMN:[21] The synthetic process was similar to TPMN except for the change of starting materials. ^{1}H NMR (400 MHz, $CDCl_3$): 7.72 (s, 1H), 7.65 (d, J = 4 Hz, 1H), 7.47 (d, J = 8.8 Hz, 2H), 7.28 (d, J = 4 Hz, 1H), 7.09–7.11 (m, 4H), 6.86–6.89 (m, 6 H), and 3.81 (s, 6H). ^{13}C NMR (100 MHz, $CDCl_3$): 157.74, 156.83, 150.76, 150.13, 140.50, 139.40, 132.60, 127.51, 127.44, 123.04, 122.73, 118.75, 114.94, 114.72, 113.82, 74.27, and 55.48. ESI HRMS: calcd. for $C_{28}H_{21}N_3O_2S$ $[M]^+$: 463.1354, found: 463.1381.

[CCDC 1562093 contains the supplementary crystallographic data for this paper. These data can be obtained free of charge from The Cambridge Crystallographic Data Centre via www.ccdc.cam.ac.uk/data_request/cif.].

Supporting Information

Supporting Information is available from the Wiley Online Library or from the author.

Acknowledgements

D.W. and H.S. contributed equally to this work. This work was partially supported by the National Basic Research Program of China (973 Program; Grant Nos. 2013CB834701 and 2013CB834702), the University Grants Committee of Hong Kong (Grant No. AoE/P-03/08), the Research Grants Council of Hong Kong (Grant Nos. 16301614, 16305015, and N_HKUST604/14), Innovation and Technology Commission (Grant No. ITC-CNERC14SC01), the National Science Foundation of China (Grant Nos. 81372274, 81501591, and 8141101080), the Science and Technology Planning Project of Guangdong Province (Grant Nos. 2014A030313033 and 2014A050503037), and the Shenzhen Science and Technology Program (Grant Nos. JCYJ20130402103240486 and JCYJ20160509170535223). B.Z.T. is also grateful for the support from the Guangdong Innovative Research Team Program of China (Grant No. 201101C0105067115). All the procedures used in this study with Zebrafish were performed in accordance with the guidelines and regulations set out by the Animal Ethics Committee of the Hong Kong University of Science and Technology (HKUST).

Conflict of Interest

The authors declare no conflict of interest.

Keywords

aggregation-induced emission, facile synthesis, lipid droplet-specific imaging, photodynamic therapy, red/NIR emission

Received: July 19, 2017
Revised: August 16, 2017
Published online:

[1] a) B. N. G. Giepmans, S. R. Adams, M. H. Ellisman, R. Y. Tsien, *Science* **2006**, *312*, 217; b) T. Terai, T. Nagano, *Curr. Opin. Chem. Biol.* **2008**, *12*, 515.

[2] a) D. W. Domaille, E. L. Que, C. J. Chang, *Nat. Chem. Biol.* **2008**, *4*, 168; b) R. Y. Tsien, *Angew. Chem., Int. Ed.* **2009**, *48*, 5612; c) M. Y. Hu, L. Li, H. Wu, Y. Su, P. Y. Yang, M. Uttamchandani, Q. H. Xu, S. Q. Yao, *J. Am. Chem. Soc.* **2011**, *133*, 12009.

[3] a) C. K. Lim, S. Kim, I. C. Kwon, C. H. Ahn, S. Y. Park, *Chem. Mater.* **2009**, *21*, 5819; b) K. Y. Pu, K. Li, B. Liu, *Adv. Funct. Mater.* **2010**, *20*, 2770; c) A. Shao, Y. Xie, S. Zhu, Z. Guo, S. Zhu, J. Guo, P. Shi, T. D. Jame, H. Tian, W. Zhu, *Angew. Chem., Int. Ed.* **2015**, *54*, 7275; d) Y. Gao, G. Feng, T. Jiang, C. Goh, L. Ng, B. Liu, B. Li, L. Yang, J. Hua, H. Tian, *Adv. Funct. Mater.* **2015**, *25*, 2857; e) H. Lu, Y. Zheng, X. Zhao, L. Wang, S. Ma, X. Han, B. Xu, W. Tian, H. Ga, *Angew. Chem., Int. Ed.* **2016**, *55*, 155.

[4] J. B. Birks, *Photophysics of Aromatic Molecules*, Wiley, London, UK **1970**.

[5] J. Luo, Z. Xie, J. W. Y. Lam, L. Cheng, H. Chen, C. Qiu, H. S. Kwok, X. Zhan, Y. Liu, D. Zhu, B. Z. Tang, *Chem. Commun.* **2001**, 1740.

[6] a) J. Mei, N. L. C. Leung, R. T. K. Kwok, J. W. Y. Lam, B. Z. Tang, *Chem. Rev.* **2015**, *115*, 11718; b) J. Mei, Y. Hong, J. W. Y. Lam, A. Qin, Y. Tang, B. Z. Tang, *Adv. Mater.* **2014**, *26*, 5429.

[7] a) Q. Zhao, S. Zhang, Y. Liu, J. Mei, S. Chen, P. Lu, A. Qin, Y. Ma, J. Z. Sun, B. Z. Tang, *J. Mater. Chem.* **2012**, *22*, 7378; b) Z. Zhao, H. Su, P. Zhang, Y. Cai, R. T. K. Kwok, Y. Chen, Z. He, X. Gu, X. He, H. H. Y. Sung, I. D. Williams, J. W. Y. Lam, Z. Zhang, B. Z. Tang, *J. Mater. Chem. B* **2017**, *5*, 1650.

[8] W. Qin, K. Li, G. Feng, M. Li, Z. Yang, B. Liu, B. Z. Tang, *Adv. Funct. Mater.* **2014**, *24*, 635.

[9] W. Qin, D. Ding, J. Liu, W. Z. Yuan, Y. Hu, B. Liu, B. Z. Tang, *Adv. Funct. Mater.* **2012**, *22*, 771.

[10] D. J. Murphy, *Prog. Lipid Res.* **2001**, *40*, 325.

[11] a) S. Martin, R. G. Parton, *Nat. Rev. Mol. Cell Biol.* **2006**, *7*, 373; b) H. Zhang, Y. Wang, J. Li, J. Yu, J. Pu, L. Li, H. Zhang,

S. Zhang, G. Peng, F. Yang, P. Liu, *J. Proteome Res.* **2011**, *10*, 4757; c) A. W. Cohen, B. Razani, W. Schubert, T. M. Williams, X. B. Wang, P. Iyengar, D. L. Brasaemle, P. E. Scherer, M. P. Lisanti, *Diabetes* **2004**, *53*, 1261.

[12] K. G. M. Alberti, P. Zimmet, J. Shaw, *Lancet* **2005**, *366*, 1059.

[13] A. Loudet, K. Burgess, *Chem. Rev.* **2007**, *107*, 4891.

[14] P. M. Gocze, D. A. Freeman, *Cytometry* **1994**, *17*, 151.

[15] K. Yen, T. T. Le, A. Bansal, S. D. Narasimhan, J. X. Cheng, H. A. Tissenbaum, *PLoS One* **2010**, *5*, e12810.

[16] a) M. Kang, X. Gu, R. T. K. Kwok, C. W. T. Leung, J. W. Y. Lam, F. Li, B. Z. Tang, *Chem. Commun.* **2016**, *52*, 5957; b) M. Gao, H. Su, Y. Lin, X. Ling, S. Li, A. Q, B. Z. Tang, *Chem. Sci.* **2017**, *8*, 1763; c) M. Jiang, X. Gu, J. W. Y. Lam, Y. Zhang, R. T. K. Kwok, K. S. Wong, B. Z. Tang, *Chem. Sci.* **2017**, *8*, 5440.

[17] a) J. P. Celli, B. Q. Spring, I. Rizvi, C. L. Evans, K. S. Samkoe, S. Verma, B. W. Pogue, T. Hasan, *Chem. Rev.* **2010**, *110*, 2795; b) M. Ethirajan, Y. Chen, P. Joshi, R. K. Pandey, *Chem. Soc. Rev.* **2011**, *40*, 340; c) Q. Hu, M. Gao, G. Feng, B. Liu, *Angew. Chem., Int. Ed.* **2014**, *53*, 14225; d) E. Zhao, H. Deng, S. Chen, Y. Hong, C. W. Leung, J. W. Lam, B. Z. Tang, *Chem. Commun.* **2014**, *50*, 14451; e) Y. Yuan, C. J. Zhang, M. Gao, R. Zhang, B. Z. Tang, B. Liu, *Angew. Chem., Int. Ed.* **2015**, *54*, 1780.

[18] a) R. K. Shiroodi, V. Gevorgyan, *Chem. Soc. Rev.* **2013**, *42*, 4991; b) C. M. R. Volla, I. Atodiresei, M. Rueping, *Chem. Rev.* **2014**, *114*, 2390; c) I. Wheeldon1, S. D. Minteer, S. Banta, S. C. Barton, P. Atanassov, M. Sigman, *Nat. Chem.* **2016**, *8*, 299.

[19] a) I. S. Mian, C. Rose, *Integr. Biol.* **2011**, *3*, 350; b) H. Hillebrand, F. Watermann, R. Karez, U.-G. Berninger, *Oecologia* **2001**, *126*, 114.

[20] O. Pelkonen, M. Turpeinen, *Xenobiotica* **2007**, *37*, 1066.

[21] Y. Li, T. Ren, W.-J. Dong, *J. Photochem. Photobiol., B* **2013**, *251*, 1.